Journal of Environmental Management 279 (2021) 111685

Contents lists available at ScienceDirect

Journal of Environmental Management

journal homepage: http://www.elsevier.com/locate/jenvman

Research article

Structural and elemental analysis of biochars in the search of a synthetic path to mimetize anthropic Amazon soils

Sugandha D. Pandey [a,b,c,1,**], Fernanda G. Mendonça [b,1,*], Marcio N. Rodrigues [d], Beatriz P. Z. Faria [c], João L.E. Campos [a], Igor F.P.C. Noronha [b], Sara S. Vieira [b], Nadiene A.V. Santos [e], Luiz A. Fernandes [d], Regynaldo A. Sampaio [d], Fernando Colen [d], Zuy M. Magriotis [f], Ado Jorio [a,***]

[a] Departamento de Física, ICEx, Universidade Federal de Minas Gerais, Av. Antônio Carlos, 6627, 31.270-901, Belo Horizonte, MG, Brazil
[b] Departamento de Quimica, ICEx, Universidade Federal de Minas Gerais, Av. Antônio Carlos, 6627, 31.270-901, Belo Horizonte, MG, Brazil
[c] Departamento de Engenharia, DESA, Universidade Federal de Minas Gerais, Av. Antônio Carlos, 6627, 31.270-901, Belo Horizonte, MG, Brazil
[d] Instituto de Ciências Agrárias, Universidade Federal de Minas Gerais, Av. Universitária, 1000, 39404-547, Montes Claros, MG, Brazil
[e] Departamento de Química, Instituto de Ciências Naturais, Universidade Federal de Lavras, Av. Doutor Sylvio Menicucci, 1001 - Kennedy, 37200-900, Lavras, MG, Brazil
[f] Departamento de Engenharia, Escola de Engenharia, Universidade Federal de Lavras, Av. Doutor Sylvio Menicucci, 1001 - Kennedy, 37200-900, Lavras, MG, Brazil

ARTICLE INFO

Keywords:
Biochar
Terra preta de índio
Carbon
Raman spectroscopy
Chemical activation

ABSTRACT

In this work, chemical and structural properties of various biochars were analyzed and compared with those from a highly stable anthropic soil, *Terra Preta de Índio* (TPI). TPI is believed to be responsible for the fertility of Amazonian soils and their stability; therefore, the production of a synthetic TPI would be of great interest for agricultural applications. Biochar produced from different raw biomasses were comprehensively characterized and, based on the obtained results, a preliminary study was performed testing three different routes of chemical activation using nitric acid, phosphoric acid, and potassium hydroxide as activating agents. After chemical activations, metal contents in the biochars decreased, as expected, and high degrees of carbonization were observed. In the case of the activation performed with HNO_3, intense signals related to carboxylic groups in TG-MS analysis and in potentiometric titrations point out to a highly oxygenated biochar. Structural analysis showed that activations generated point defects in sp^2-carbon structures of biochar, with the material obtained after KOH activation showing a high surface area (569 $m^2\ g^{-1}$), an important feature for the use as soil amendment.

1. Introduction

Terra Preta de Índio (TPI, in English: Indian black earth) is a denomination of an anthropic Amazonian soil rich in carbon that presents black color and arises from the decomposition of waste and burning of biomass promoted by ancient indigenous civilization. It is believed that TPI is responsible for the high fertility and stability of Amazonian anthropic soils (Glaser and Birk, 2012), presenting promising applications in agriculture.

It is known that sp^2 and sp^3-carbons in TPI arise from structures between nanographite and amorphous carbon, named as stages 1 and 2 of carbon amorphization (Archanjo et al., 2014; Jorio et al., 2012; Pagano et al., 2016; Ribeiro-Soares et al., 2013). Archanjo et al. (2015) and Ribeiro-Soares et al. (2013) showed that the surface of the grains in TPI presents a graphitic structural disorder, therefore being more reactive towards the adsorption and desorption of nutrients, while the inner part would be responsible for its stability.

One of the main current challenges is to artificially reproduce the agricultural properties of the anthropic TPI. In the search for a synthetic route to obtain a material that presents similar structural and elemental characteristics when compared to TPI, which could be further used as soil amendment, biochar appears as a promising alternative. Biochar is

* Corresponding author. Departamento de Química, ICEx, Universidade Federal de Minas Gerais, Av. Antônio Carlos, 6627, 31.270-901, Belo Horizonte, MG, Brazil
** Corresponding author. Departamento de Física, ICEx, Universidade Federal de Minas Gerais, Av. Antônio Carlos, 6627, 31.270-901, Belo Horizonte, MG, Brazil
*** Corresponding author. Departamento de Física, ICEx, Universidade Federal de Minas Gerais, Av. Antônio Carlos, 6627, 31.270-901, Belo Horizonte, MG, Brazil
E-mail addresses: sugandha.dogra@gmail.com (S.D. Pandey), nandagm@ufmg.br (F.G. Mendonça), adojorio@fisica.ufmg.br (A. Jorio).
[1] These authors contributed equally to this work.

https://doi.org/10.1016/j.jenvman.2020.111685
Received 6 June 2020; Received in revised form 21 October 2020; Accepted 15 November 2020

the solid product obtained in the pyrolysis of biomass, a thermochemical process that occurs in the absence of oxygen, usually performed to obtain biofuels (Huber et al., 2006). Its composition consists on organic compounds non-converted during pyrolysis, carbon residues produced by the decomposition of biomass, besides a mineral fraction containing mainly Ca, K and Mg (Huber et al., 2006; Kan et al., 2016). Moreover, biochars usually present a fraction of oxygenated functional surface groups, which characteristics will depend upon the pyrolysis temperature and on the raw biomass (Bai et al., 2020; Dominguez et al., 2020; Jaganathan and Varunkumar, 2020; Salam et al., 2020; Yang et al., 2006).

Previous works showed that biochar can be used as soil amendment leading to an increase of the carbon content in the soil, besides acting in the sorption of organic and inorganic contaminants by reducing their mobility in contaminated soils (Bashir et al., 2020; Gámiz et al., 2019; Kavitha et al., 2018; Xiao et al., 2019). Aiming to increase the content and characteristics of surface groups in biochars or to enhance their surface area, chemical activation can be performed. The literature describes several ways of obtaining activated and functionalized biochars, *e.g.* the oxidation with nitric or phosphoric acids and potassium hydroxide (Boguta et al., 2019; El-Banna et al., 2018; Martínez-Casillas et al., 2018; Sullivan et al., 2019; Wang et al., 2019). After functionalization, biochars generally present a significative amount of oxygenated functional surface groups and higher volume of pores with concomitant development of surface area (Q. Chen et al., 2018; Martínez-Casillas et al., 2018). Therefore, an increase on the ionic exchange capacity is observed for chemical activated biochars enabling better performance in different applications, such as adsorption of toxic metals and contaminants in aqueous media (Chen et al., 2019; T. Chen et al., 2018; Cuong et al., 2019; Ma et al., 2019; Shang et al., 2018; Wang et al., 2020), besides as an electrode material for supercapacitors (Martínez-Casillas et al., 2018).

Herein, we performed the characterization of biochars produced from several different raw biomasses and compared the results with those obtained from TPI. Physical, chemical, and structural characterizations were performed to provide the basic information of carbonized biomass material in comparison to the carbon fraction present in TPI-soil (TPI-carbon), guiding us to the production of biochar similar to TPI. Subsequently, a preliminary activation of a biochar sample was performed in three different routes, using nitric and phosphoric acids, and potassium hydroxide as activating agents. The obtained biochars were characterized to unveil a pathway that can guide us into the best route in order to obtain a synthetic material presenting structural and elemental characteristics as close as possible to TPI.

2. Materials and methods

2.1. Samples and preparation methods

TPI-soils samples were collected from the bank of Lago Sapucuá, in the lower Trombetas River basin, a tributary of Amazonas River, Pará state, Brazil (Lat. 1° 80′78″ S Long. 56°05′31″ W). We collected TPI samples from five different locations in a site considered to be an area of good crop production, thus named as TPI-1, TPI-2, TPI-3, TPI-4 and TPI-5. Biochars (BC) were prepared from castor beans presscake (CBP), sugarcane bagasse (SB), pequi shell (PS) and sewage sludge (SS), under different pyrolysis temperatures. The conditions of pyrolysis were evaluated and predetermined in previous works (Santos et al., 2017; Zelaya et al., 2019). BC from CBP, from now on named BC-CBP, were produced from *Ricinus communis* L. seeds after oil extraction to biodiesel production. Four different BCs were produced from the fast pyrolysis of CBP at 300 (BC-CBP-I), 400 (BC-CBP-II), 500 (BC-CBP-III) and 600 °C (BC-CBP-IV) in a pyrolizer with a low oxygen content under nitrogen flow at the Laboratory of Catalysis and Biofuels in the Federal University of Lavras, MG, Brazil. BC-SB was produced from *Saccharum officinarum* L. stalks after mechanical extraction of the juice, by slow pyrolysis at 350 °C for 2 h. BC-PS was produced from *Caryocar brasiliense* Camb. shell (pequi, a native fruit from Brazilian Savanna) after removal of the seeds, by slow pyrolysis at 450 °C. SS was collected from Montes Claros' municipal wastewater treatment plant in the state of Minas Gerais, Brazil, which receives and treat only domestic sewage. Then, two different BC-SS were produced by slow pyrolysis at 450 °C (BC-SS-I) and 350 °C (BC-SS-II). These BCs were produced at the Institute of Agricultural Sciences from the Federal University of Minas Gerais (UFMG).

Chemical activations of BC-CBP-II were realized in three different routes, using nitric acid (HNO_3), phosphoric acid (H_3PO_4) or potassium hydroxide (KOH) as activating agents. The activation agents were selected based on previous work reported in the literature (Boguta et al., 2019; El-Banna et al., 2018; Martínez-Casillas et al., 2018; Sullivan et al., 2019; Wang et al., 2019). The activation with HNO_3 was performed according to the procedure described by Barrera et al. (2018). 15 mL of concentrated HNO_3 was added to 500 mg of BC-CBP-II under heating in reflux at 80 °C during 5, 15 and 30 min, to originate BN5, BN15 and BN30, respectively. Afterward, the samples were washed with abundant distilled water up to pH 7 to remove the excess of acid and water-soluble products of oxidation. After washing, materials were dried at 80 °C for 18 h. H_3PO_4 activation was performed based on Sun et al. (2018), in which 500 mg of BC-CBP-II was impregnated with 10 mL of an aqueous solution of H_3PO_4 at weight ratios of 1:1 and 1:2 for 24 h, originating BP1.1 and BP1.2, respectively. The mixtures were dried and thermally treated under nitrogen atmosphere at 500 °C for 90 min, then washed with abundant distilled water and dried at 80 °C overnight. In the case of activation with KOH, based on Martínez-Casillas et al. (2018), BC-CBP-II and KOH were mechanically mixed in weight ratios of 1:1 (BK1.1) and 1:2 (BK1.2), and the mixtures were thermally treated under nitrogen atmosphere at 500 °C for 90 min. The activated samples were washed with an HCl solution at 20%, distilled water, and dried at 80 °C for 18 h.

2.2. Characterization methods

Elemental composition analyses of TPI-soil and all BCs were carried out in the Institute of Agricultural Sciences of UFMG, Montes Claros. Chemical analyses were performed in replicates and repeated to confirm the results, which refer to the total concentrations of the elements. Total carbon was calculated using wet digestion on potassium dichromate method. Total nitrogen was determined using the Kjeldahl method (Tedesco et al., 1995). For determination of total contents of P, K, Ca, Mg, Fe, Cu, Zn, Mn, Cr, Ni, and Pb, open digestion was performed with 3:1 nitric-perchloric solution in a digester block. P was quantified using a UV–Vis spectrophotometer (Nova 1600) and K was determined in a flame photometer (Micronal B 462). The other elements were analyzed by atomic absorption spectrometry in a Varian AAS 240 F S spectrometer according to Malavolta (2006).

Surface topographies of TPI-carbon and BCs were analyzed by scanning electron microscopy (SEM) in a Dual Beam electron microscope and the quantitative elemental composition by energy-dispersive X-ray spectroscopy (EDXS) in an Esprit Bruker Nano GmbH equipment with primary energy of 15kev. TPI-carbon or black grains were picked manually under a microscope by placing small measure (~1 mg) of TPI-soil on a glass slide.

Thermogravimetric analyses (TGA) of BCs and TPI-soil were carried out in a Shimadzu TGA-60 thermobalance under air atmosphere (50 mL min^{-1}) with a heating rate of 10 °C min^{-1}. Infrared spectra (IR) were recorded in a Bruker ALPHA equipment in the wavelengths between 4000 and 400 cm^{-1} with 64 scans per sample and spectral resolution of 2 cm^{-1}, with samples ground in KBr in a 1:100 ratio.

Raman experiments were carried out on BCs and TPI-carbon in an Andor TM Technology-shamrock sr-303i spectrometer coupled with a charge-coupled device detector, in the backscattering configuration using 60x oil immersion objective lens. Excitation was provided by 488 nm (2.54 eV) laser with the exposure time 60 s on each sample. A Neon

lamp was used to calibrate the spectra for spectral range (505 nm–643 nm). Raman spectra were also acquired with WITec Raman spectrometer using 457 and 532 nm laser lines. Raman data were analyzed utilizing parametrized principal component analysis (PCA) (Campos et al., 2018) (details of PCA are described in SI).

Total reflection X-ray fluorescence (TXRF) spectroscopy measurements were carried out using an S2 PICOFOX benchtop spectrometer Bruker Nano GmbH, equipped with a molybdenum tube – Kα line 17.5 keV excitation source (600 A, 50 kV, 50 W), a multi-layer monochromator with layer system made of 100 Ni/C duplicate layers with a spacing of 2.88 nm, and a silicon drift detector with 10 mm^2 active area. Detector's resolution was better than 160 eV at 10 kpcs (for Mn K line). Processing of the X-ray spectra and composition determination were performed using the SPECTRA software, version 7.0 (Bruker Nano GmbH) (details of sample preparation are described in SI).

Thermogravimetric-mass spectrometry analyses (TG-MS) were performed in a NETZSCH equipment model STA 449 F3, coupled to a mass spectrometer NETZSCH Aëolos model QMS 403 C. It was used about 15 mg of the samples under an argon flow (20 mL min^{-1}), up to 900 °C in a heating rate of 5 °C min^{-1}. Carbon, hydrogen and nitrogen contents were determined through elemental analysis in a Series II–CHNS/O 2400 PerkinElmer Elemental Analyzer.

Potentiometric titrations were performed in a SHOTT automatic titrator (Titroline 7000) with a combined pH electrode model N6280 (SHOTT), under a nitrogen atmosphere. For titrations, 50 mg of sample was dispersed in 20 mL of a 0.0021 mol L^{-1} HCl solution and titrated with a CO_2-free solution of NaOH (0.0152 mol L^{-1}). To keep the H^+ ion activity constant during the experiments, ionic strengths of the HCl and NaOH solutions were fitted to 0.10 mol L^{-1} by dissolution of sodium chloride. To determine the nature and amount of the acidic functional groups present on the surface of the samples a non-linear regression program was used (Alves et al., 2016; Lemos et al., 2013).

Specific surface area was determined by nitrogen adsorption using Brunauer, Emmett and Teller method (BET) with N_2 adsorption/desorption in an Autosorb 1 Quantachrome instrument, with degassing at 200 °C for 8 h before analysis.

3. Results and discussions

3.1. Biochar physical, chemical, and structural properties

Physical, chemical and structural characterizations were performed to provide basic information of biochars in comparison to TPI-carbon, guiding us to the production of BC similar to TPI. Elemental composition of TPI-soil samples showed a comparable pattern of elements as it was observed by Pagano et al. (2016), despite the different locations (Table S1 in the support information). Organic carbon (OC) concentration is low in TPI-soil due to the sandy texture and agricultural use of TPI soils, which favored the organic matter mineralization. Nitrogen content is also low probably as a result of the loss of N–NO_3 by leaching and/or N–NH_3 by volatilization. Interestingly, high values were obtained for P content, which is believed to be related to the process of slash and burning, common practices of the locals.

According to the elemental composition of all BC prepared (Table S2), biochars produced from plant residues had a higher OC content than those produced from SS, what can be explained by the presence of long carbon chain compounds in plants such as lignin and cellulose. It is noteworthy that some heavy metals such as Cr, Ni, Zn, Cu and toxic heavy metal Pb are present in a slightly higher concentration in BC-SS-I and BC-SS-II. Nonetheless, the values are much lower than the allowed limit (CONAMA, 2006), as expected, since this SS was collected at a wastewater treatment plant that receives and treats only domestic sewage. In this work, the carbon structure of the biochars obtained from SS will not depend on these extremely low amounts of heavy metals, as it will be shown in Raman spectra; however, its determination is certainly important for safety in case of real use in any environmental or agricultural application.

Qualitative elemental composition using EDXS (Fig. 1) showed general trends similar to the results presented in Tables S1 and S2, despite the different techniques used and issues with the homogeneity of samples, as EDXS analyses only a tiny amount of material. EDXS showed that the composition of TPI and BCs has a major contribution coming from C and O, besides Al and Si (Fig. 1a and c). BC-SB, BC-SS-I and TPI-carbon presented higher Si content, which plays an important role in protecting the cell wall of plants against pests and pathogens (Filgueiras, 2007). EDXS also showed the presence of Ca and Mg (Fig. 1b), which are good exchangeable cations and are responsible for the increase in effective cation exchange capacity of the soil, what could lead to an improvement on soil conditioning (Sharma et al., 2015). In the case of BC-PS, its composition is essentially based on C and O, with small amounts of K, Cl, Mg, and P. It is notable the presence of phosphorus (P) and potassium (K) in all BCs and TPI-carbon, which are important macronutrients for soil fertility, even in small quantities. The higher percentage of these nutrients in TPI-carbon possibly results from continual incorporation of organic products by Amerindians (Bezerra, 2015; Glaser et al., 2001). Major and minor elemental composition of BC-CBPs (Fig. 1c and d) showed there is an increase on the content of elements such as Si and Ca when pyrolysis temperature increases from 300 to 600 °C, what can also be observed for Mg, P, and K contents for most of the materials. This behavior was expected since these metals could not be burned under the pyrolysis conditions, unlike carbonaceous material, especially more amorphous carbon.

To examine the topography and morphology of TPI-carbon and produced BCs, SEM images were obtained (Figure S1). SEM images of BC-SB showed a non-uniform fibrous structure (Figure S1a), with most grains presenting tube-shaped pores similar to hives, a format inherited from the tissue of the precursor plant. The pores, due to their size and shape, serve as a gateway for adsorbents (Suliman et al., 2016). This type of structure can retain nutrients in the soil and give structural conditioning because of its morphology. SEM images of BC-CBP samples (Figures S1b-e) showed that these materials are apparently homogeneous and present fibrous structure as well. Morphological changes were observed with thermal treatment, as porosity apparently increased with pyrolysis temperature when comparing SEM images of BC-CBP-I and II (Figures S1b,c) with BC-CBP-III and IV (Figures S1d,e). For BC-PS (Figure S1f), it is possible to observe heterogeneous grains and a fibrous structure with pores of an irregular pattern. In the case of BC-SS samples, both showed irregular patterns as expected for a mixture of organic matter and mineral residues, with grains presenting a sandy morphology (Figures S1g,h). The morphologies of produced BC were compared with TPI-carbon (Figure S1i), which presents various grain shapes, generally nonspherical, and a porous morphology as previously reported (Jorio et al., 2012).

TGA curve obtained for TPI-soil showed a small weight loss observed before 100 °C, probably related to the loss of adsorbed water, with a second weight loss at 300 °C, related to carbon oxidation (Fig. 2a). At the end of the analysis, i.e., at 900 °C, TPI showed a total weight loss of only 12%, what can indicate a high amount of inorganic matter present in this material coming from the soil, which is not burned under oxidizing conditions. For BCs, it can be observed that BC-SB, BC-PS and BC-CBP-II presented very similar curves (Fig. 2a). The most significant weight loss for these materials was observed at approximately 400 °C, which is probably related to carbon oxidation by O_2, forming CO_2. On the other hand, the TGA curve obtained for BC-SS-I presented a weight loss starting at approximately 300 °C, a relatively lower temperature when compared to the other BCs. This is probably associated with a greater amount of amorphous carbon, with a high amount of residual mass (ashes, 60%), indicating high content of inorganic matter. The residual mass is related to the presence of metals and other inorganic contaminants and due to the presence of clay (particles with average diameter <0.002 mm) mixed with the organic matrix in SS (Braga et al., 2020). The amount of insoluble mineral waste in SS may be in the order of 35%,

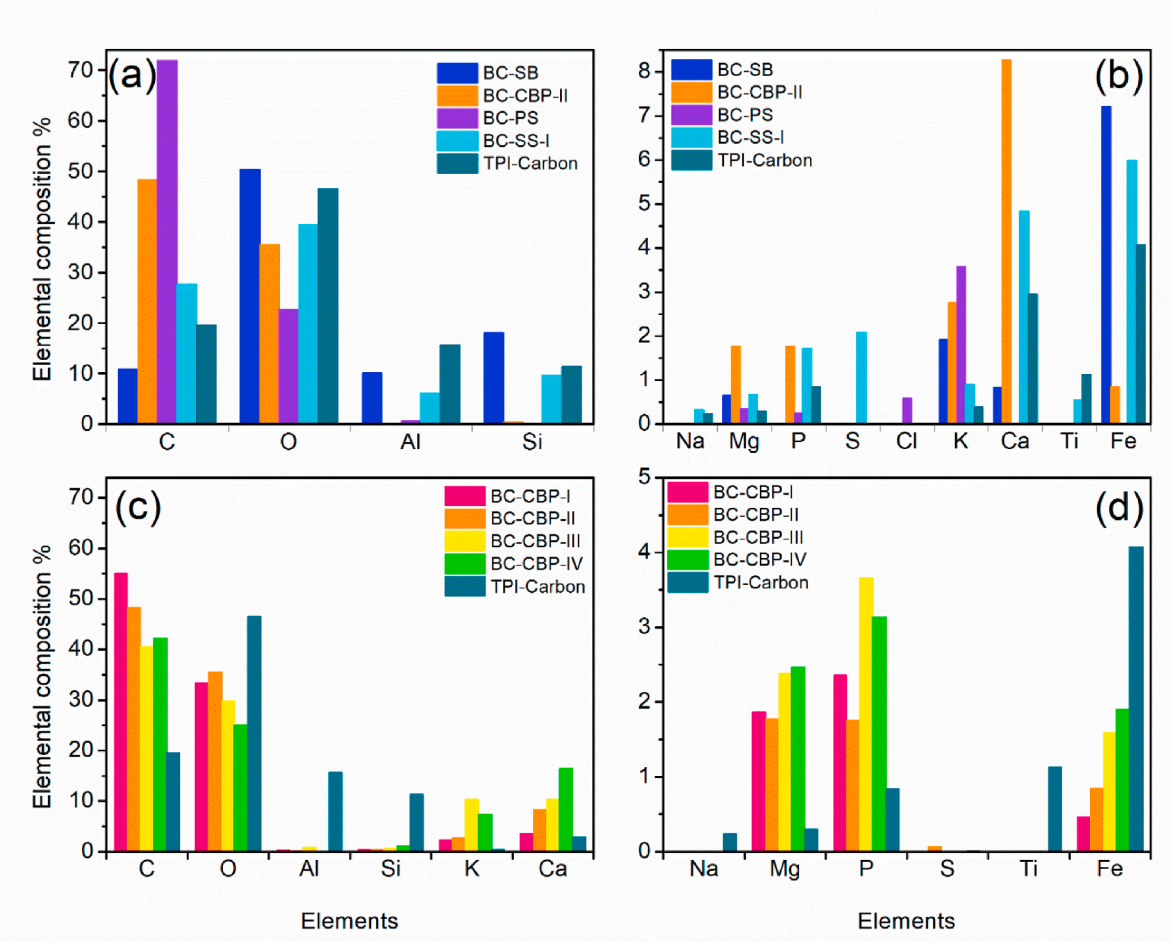

Fig. 1. (a) Major and (b) minor elemental composition of BC- SB, BC-CBP-II, BC-PS, BC-SS-I and TPI-carbon, respectively (results obtained for BC-SS-II are very similar to those from BC-SS-I and they are not shown here to improve figure readability). (c) Major and (d) minor elemental composition of all BC-CBP prepared at 300–600 °C and TPI-carbon.

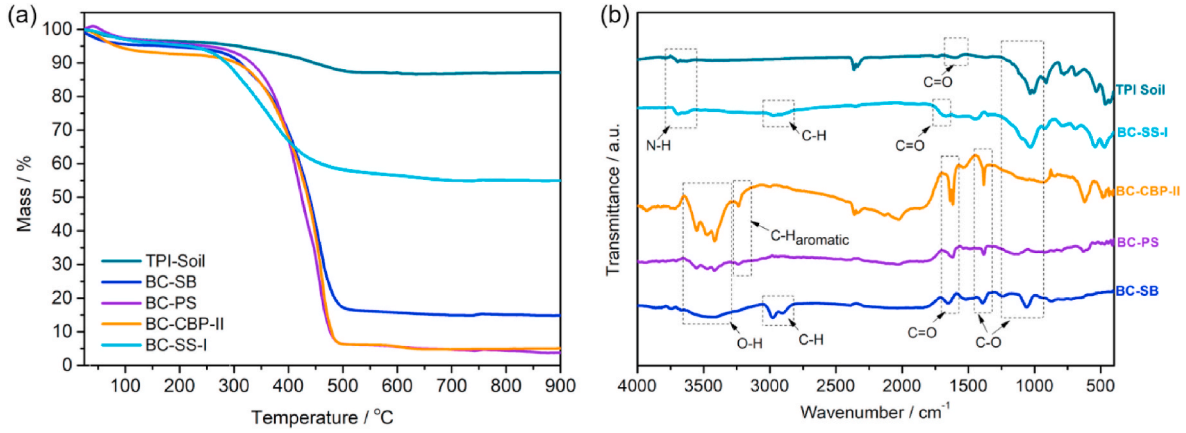

Fig. 2. (a) TGA curves (in air) and (b) IR spectra obtained for TPI-soil, BC-SB, BC-PS, BC-CBP-II, and BC-SS-I.

which explains the similarity between TGA curves obtained for TPI-soil and BC-SS-I (see Figure S2 for all TGA curves).

The different raw biomasses containing various functional groups also generated distinct IR spectra for each material, as depicted in Fig. 2b. The spectrum obtained for TPI-soil presents bands between 3700 and 3615 cm^{-1} related to N–H bond stretching, besides C═O stretching near 1600 cm^{-1} and C–O stretching at 1036 and 1006 cm^{-1}. The bands observed in 2360 and 2340 cm^{-1} are related to C═O stretching in CO_2 from air. In the case of the BCs, the bands highlighted in Fig. 2b are related to N–H stretching (3700-3615 cm^{-1}), O–H stretching (3500-3400 cm^{-1}), aromatic C–H vibrations (3230 cm^{-1}), C–H stretching (2980-2900 cm^{-1}), C═O stretching (1680-1620 cm^{-1}), and C–O stretching (1385 cm^{-1}; 1200-1080 cm^{-1}). The spectra indicate that BC-SB, BC-PS and BC-CBP-II are composed essentially by carbon and oxygenated functional groups, as expected for lignocellulosic biomass derivatives. It is possible to observe that the spectrum obtained for BC-

SS-I is the most similar to TPI, indicating that SS biomass presents the most of functional groups which are present in TPI (see Figure S3 for all IR spectra).

Raman spectroscopy is established as one of the most powerful techniques for the characterization of structural properties of sp^2 carbon structures at the nanoscale level (Jorio et al., 2011). Fig. 3a shows the Raman spectra of TPI-carbon and BCs, where it is possible to observe that they all exhibit a similar amorphous-carbon structure, but the relative intensities of D and G bands varied in all spectra (see Figure S4 for all Raman spectra), which brings detailed information on the degree of amorphization (Campos et al., 2018; Jorio et al., 2012; Pagano et al., 2016; Ribeiro-Soares et al., 2013). The observed Raman signal of TPI-carbon and BCs majorly comes from sp^2-hybridized carbon-like structure, although we cannot rule out the presence of sp^3 hybridization, as visible light excites mostly sp^2 π electron bands (Jorio et al., 2012). Structural analyses of sp^2-hybridized carbon of all BCs and TPI-carbon using the carbon-structure-parametrized PCA (Fig. 3b) (Campos et al., 2018) displayed that BC prepared from SS have greater similarity with TPI-carbon concerning the sp^2 carbon structural nature of the BCs. The sp^2 carbon structure in TPI is believed to be responsible for its high stability associated with a high ion exchange capacity (Jorio et al., 2012).

In more details, the first principal component (PC1, x-axis) in Fig. 3b displays the divergence of data in a small region, which explains the nature of amorphous carbon present in different materials. Our parametrized PC analysis is based on sp^2-hybridized carbon with different and well-controlled degree of disorder (Campos et al., 2018), which changes the size of sp^2-carbon nanocrystallites and the number of defects in the structure. In comparison to highly-ordered sp^2-carbon structures (graphene/graphite), which lies in the positive region of the x-axis (Campos et al., 2018), the position of BCs and TPI-carbon indicates their mixed sp^2-sp^3 carbon bond nature, with small (nanometer in size) clusters of sp^2-carbon material (Jorio et al., 2012; Ribeiro-Soares et al., 2013). It can be observed that BCs prepared from plant residues are on the right side of Fig. 3b, while BC prepared from SS is closer to TPI-carbon. We can conclude that BCs prepared from plant residues present a less amorphous character in comparison to BC prepared from SS, confirming TGA results (Fig. 2a). As TPI-carbon lies on the left side of Fig. 3b, showing more amorphous character, it is consistent to consider that TPI is formed by a highly reactive carbon material, with the presence of smaller sp^2-carbon crystallites, with more defective structure and nutrients.

3.2. Activation of biochar

Taking into account that the amorphization structure of BC plays an important role on stability and reactivity of the soil, we decided to study the possibility of producing a synthetic TPI-carbon by activating the BC produced from other sources.

Considering the BCs analyzed here, we chose to face the challenge to obtain a material similar to TPI starting from one of the BC-CBP samples, investigating different routes of chemical functionalization. This decision was based on the PC analysis (Fig. 3b), which showed that BC-CBP materials are the farthest from TPI-carbon from the BC structure point of view; nevertheless, this study would allow us to screen different possibilities of functionalization and point out directions that could be applied to the other BCs previously characterized in this work, which can be further applied to several biochars coming from different raw materials.

A judicious analysis of the data presented previously in Fig. 3b enabled the evaluation of the influence of temperature on the amorphization degree of BCs produced from castor beans presscake, BC-CBP (Figure S5). The carbon-structure-parametrized PCA (Campos et al., 2018) displayed that BC-CBP-I and II are quite similar concerning the sp^2 carbon structure, while BCs obtained at 500 and 600 °C present more point defects in sp^2-carbon structures, as the data related to BC-CBP-III and IV departed along the PC2 axis in Figure S5. From the point of view of BC structure, BC-CBP-II can be considered one of the most different BCs compared to TPI-carbon. Therefore, BC-CBP-II was the chosen one to be submitted to chemical activations, in an attempt to obtain a synthetic material similar to TPI.

3.2.1. Activation of BC-CBP-II

The first investigations were performed by chemically activating BC-CBP-II on three different routes using nitric acid (HNO_3), phosphoric acid (H_3PO_4) or potassium hydroxide (KOH) as activating agents, originating seven activated BCs. We will show characterizations for one sample of each activating agent, totalizing three materials: BN30, activated with HNO_3, BP1.1, activated with H_3PO_4, and BK1.1, activated with KOH. Results for the other samples are presented in SI.

Elemental composition of activated materials (Fig. 4a; Table S3) showed that, in general, the content of metals present in activated materials was lower than the original biochar BC-CBP-II, due to acid (HNO_3/H_3PO_4) or alkaline (KOH) treatments and washing processes that the materials were submitted during their preparation (El-Banna et al., 2018; Sun et al., 2018). BP1.1 presented a higher P content compared to BC-CBP-II (Fig. 5a), showing that the treatment with H_3PO_4 was able to increase the P content, although it was not enough to reach

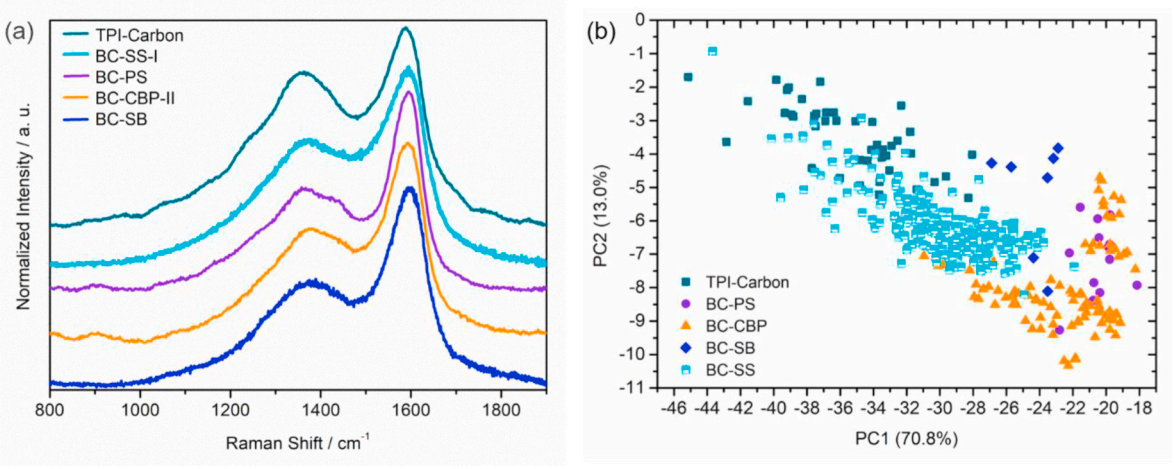

Fig. 3. (a) Raman spectra and (b) sp^2 carbon-specific parametrized PC analyses of Raman spectra obtained for BC-SB, BC-CBP-II, BC-PS, BC-SS-I, and TPI-carbon. Data obtained with 457 nm excitation laser.

(a)

	TPI	BC-CBP-II	BN30	BP1.1	BK1.1
P (g/kg)	4.2 ± 0.5	0.69 ± 0.07	0	1.6 ± 0.2	0
K (g/kg)	0.007 ± 0.001	0.32 ± 0.03	0.85 ± 0.02	3.3 ± 0.1	5.2 ± 0.1
Ca (g/kg)	1.0 ± 0.1	10 ± 1	9.04 ± 0.01	3.7 ± 0.3	3.8 ± 0.1
Mn (mg/kg)	127 ± 9	623 ± 8	1.1 ± 0.4	36 ± 2	40 ± 3

(b)

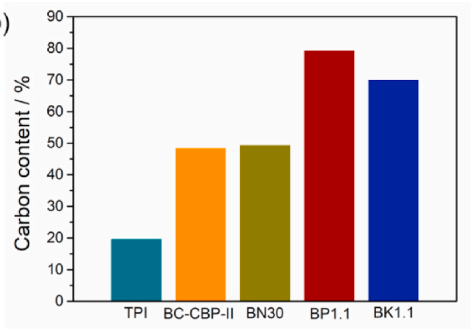

Fig. 4. (a) Elemental composition and (b) carbon content (%) obtained for TPI-soil, BC-CBP-II and activated materials. Numbers presented for TPI were obtained by averaging the values presented in Table S1. Values presented for BC-CBP-II are presented in Table S2.

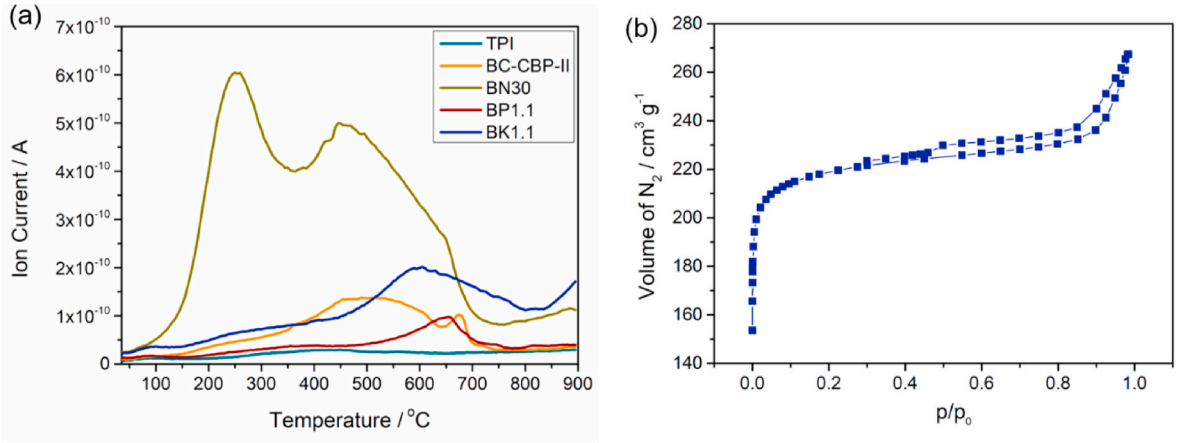

Fig. 5. (a) TG-MS curves obtained for TPI, BC-CBP-II and activated samples monitoring the evolution of *m/z* 44 (CO_2) with temperature. (b) N_2 adsorption/desorption isotherm obtained for BK1.1.

TPI. Activations decreased the K content in BC-CBP-II, except for BK1.1, in which KOH was used as an activating agent. Unexpectedly, K content was also high in BP1.1, which is probably related to the lack of homogeneity in the sample and limitations of the technique. Amounts of the exchangeable cations Ca and Mg remained in an acceptable range after activations, which would allow the produced materials to act as soil conditioners and fertilizers, for instance (Sharma et al., 2015).

Carbon contents determined for all materials (Fig. 4b; Table S4) showed that activation performed with nitric acid did not cause any considerable change in the carbon content of BC-CBP-II. Nitrogen contents in BCs treated with HNO_3 were higher than BC-CBP-II (Fig. 4b; Table S4) since this activation potentially introduces nitrogenated functional groups in biochar (Boguta et al., 2019). In the case of BP1.1 carbon content increased, and the same behavior was observed for BK1.1. These results were not expected, as activations with both H_3PO_4 and KOH were supposed to decrease the carbon content of BC (Martínez-Casillas et al., 2018; Sun et al., 2018). However, once the C/H ratio is calculated for each one of the materials (see Table S4 for H contents), an increase is observed for BP1.1 and BK1.1 compared to BC-CBP-II, what is related to a high degree of carbonization, as expected for H_3PO_4 and KOH chemical activations (Sun et al., 2018).

In order to investigate the organic functional groups present in the materials, TG-MS analyses were performed monitoring *m/z* signal 44, related to the evolution of CO_2 (Fig. 5a and S6a). The evolution of CO_2 from BCs at increasing temperatures can be related to the decomposition of organics and surface oxygenated functional groups. TPI presented a very low signal related to the loss of CO_2 ranging from 200 to 500 °C. For BC-CBP-II a more intense signal starting at approximately 150 °C was observed, related to the loss of the oxygenated groups present in this biochar. Chemical activations of BC-CBP-II led to different profiles of CO_2 loss: BN30 presented a very intense signal for CO_2, visually presenting two peaks, showing that the activation with HNO_3 produces highly oxygenated biochars, while BP1.1 and BK1.1 presented less intense peaks, emerging at higher temperatures (c.a. 600 °C). According to the literature (de la Puente et al., 1997), CO_2 evolution detected between 120 and 350 °C is related to carboxylic groups, and at higher temperatures it can be related to lactone or ester groups created during acid treatment. Monitoring of the signal related to the evolution of nitrogen monoxide (NO) for BN materials (Figure S6b) showed that the activation with HNO_3 was able to introduce either oxygenated and nitrogenated functional groups which were not previously observed in BC-CBP-II.

In order to estimate the nature and the concentration of acid functional groups, potentiometric titrations were performed for BC-CBP-II and the chemically activated samples (Figure S7). BN30 was the most oxidized sample, i.e. the one that presented the higher concentration of acid functional groups (0.006 mol g^{-1}), while BP1.1 presented the lowest amount of acid functional groups. This result is in accordance with the strength of the acids utilized as activation agents: HNO_3 is a strong acid and H_3PO_4 is a moderate acid. The results also suggest the presence of three representative functional groups in the samples: carboxylic acids (pk_a 3–6), lactones (pk_a 6–7) and phenols ($pk_a > 8$) (Alves et al., 2016; Lemos et al., 2013). Only in the case of BK1.1 groups in $pk_a < 4$ were detected, suggesting that the activation performed with KOH can originate stronger carboxylic groups during the oxidation of the biochar carbon structure.

Nitrogen adsorption-desorption analyses were performed to determine the surface areas and porosity of the materials. TPI and BN5 presented Type III isotherms, which are characteristic of multilayer adsorption (Thommes et al., 2015), with very low surface areas equal to

32 and 1.3 m^2g^{-1}, respectively (Figure S8). BC-CBP-II also presented a Type III isotherm (Figure S8) (Thommes et al., 2015), although it was not possible to calculate its surface area through the BET method using N_2 as the adsorbate. In these cases, TPI is a mesoporous sample while BC-CBP-II and BN5 are essentially macroporous, as evidenced by the obtained pore volumes and pore diameters (Table S5).

On the other hand, after chemical activation using KOH as an activating agent, the material showed a Type I(b) isotherm (Fig. 5b), characterized by a threshold that is defined from relatively low pressures, with an H4 hysteresis loop. Type I(b) isotherms are characteristic of materials that present a pore-size distribution in a wider range, including larger micropores as well as narrower mesopores (Thommes et al., 2015), as confirmed by pore diameter analysis (Figure S9; Table S5). The external surface area was determined according to the t-plot method (Lipens et al., 1964) and it was equal to 569 $m^2\ g^{-1}$, as expected for carbon materials activated with KOH (Q. Chen et al., 2018; Martínez-Casillas et al., 2018). This high surface area can be important for the application of these materials in soils, acting as good sorbents for nutrients, for instance (Ahmad et al., 2014).

Finally, Raman spectra of activated BCs were collected (Figure S10) and structural analysis of sp^2-hybridized carbon of all BC and TPI-carbon was performed using carbon-structure-parametrized PCA (Campos et al., 2018) (Fig. 6). Raman spectra showed D and G bands with variable intensities, as described for the previous BCs, coming from sp^2-hybridized carbon-like structure, not excluding the presence of sp^3 hybridization (Jorio et al., 2012). PCA showed that the performed activations were able to generate structural changes in the sp^2 carbon nature of BC-CBP-II. In the cases of BN15, BN30 and BK1.2 these changes were directed towards TPI-carbon (Fig. 6), showing that specific conditions of activation using HNO_3 or KOH yielded BCs presenting more amorphous character. For the activations with H_3PO_4, instead, the obtained materials presented less amorphous character, as BP1.1 and BP1.2 departed to the right side on Fig. 6 (PC1 axis) (Campos et al., 2018), indicating that H_3PO_4 does not lead to the desired amorphization of the carbon structures.

Therefore, concerning the structure of sp^2-hybridized carbon and the amorphization structure of BCs, three of the activation conditions investigated in this work afforded materials similar to TPI-carbon: BN15, BN30, and BK1.2. Regarding the results obtained from elemental analysis, one can envisage that the best option to obtain the most similar biochar compared to TPI can be the combination of the three activating agents investigated in this work. This could lead not only to the closest structural similarity but also to a comparable elemental composition of the produced biochar.

These conditions can be applied to other BCs produced from different raw biomasses.

4. Conclusions

We characterized biochars produced from different biomasses and compared to anthropic Amazon soils, TPI. Characterizations showed that biochar from sewage sludge and TPI-carbon displayed greater similarity in elemental composition and carbon structure. Chemical activation of biochar was studied as a method to obtain a synthetic material presenting characteristics similar to TPI. Three different routes were investigated, and characterizations of the activated BCs indicate that a combination of the methods presented herein can point towards a possible pathway to mimetize the properties of TPI in future work, when fertility tests using the activated BCs will be performed. Concerning the structure of sp^2-hybridized carbon, specific routes of activation using HNO_3 or KOH originated the most similar biochars when compared to TPI.

Credit author statement

Sugandha D. Pandey: Conceptualization, Investigation, Data curation, Visualization, Writing – original draft, Writing – review & editing. Fernanda G. Mendonça: Conceptualization, Investigation, Data curation, Visualization, Writing – original draft, Writing – review & editing. Marcio N. Rodrigues: Investigation, Data curation. Beatriz P. Z. Faria: Investigation, Data curation. João L. E. Campos: Formal analysis, Data curation. Igor F. P. C. Noronha: Investigation, Formal analysis, Data curation. Sara S. Vieira: Investigation, Formal analysis, Data curation. Nadiene A. V. Santos: Investigation. Luiz A. Fernandes: Supervision, Resources, Writing – review & editing. Regynaldo A. Sampaio: Supervision, Resources, Writing – review & editing. Fernando Colen: Supervision, Resources. Zuy M. Magriotis: Supervision, Resources. Ado Jorio: Conceptualization, Supervision, Resources, Writing – review & editing

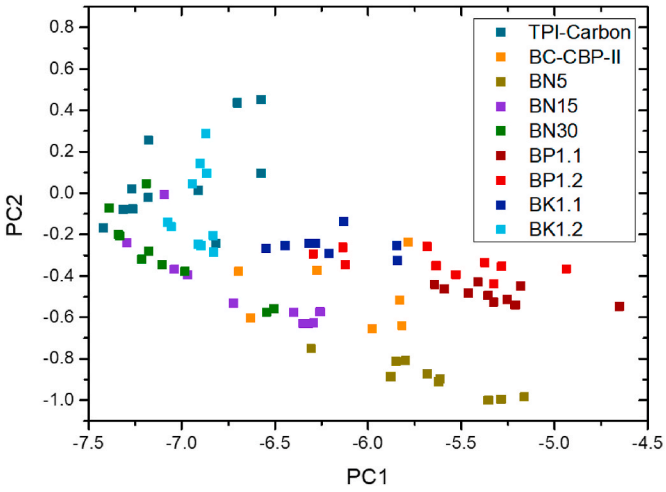

Fig. 6. sp^2-carbon specific parametrized PC analysis of the Raman spectra obtained for TPI-carbon, BC-CBP-II, and activated samples. Data obtained with 532 nm excitation laser.

Declaration of competing interest

The authors declare that they have no known competing financial interests or personal relationships that could have appeared to influence the work reported in this paper.

Acknowledgements

Authors thank the financial support from National Council for Scientific and Technological Development (CNPq): Science Without Borders, Project 401135/2014–4, Process 314731/2014–8 (S. D. Pandey); Postdoctoral Fellowship, Process 155820/2018–4 (F. G. Mendonça); Grant 302775/2018-8 (A. Jorio). The authors also thank UFMG Microscopy Center for the images obtained. To Prof. Rochel M. Lago (UFMG) for providing part of the infrastructure. To Carlos G. Bruziquesi and Prof. Luiz Carlos A. Oliveira (UFMG) for BET analyses. To Prof. João P. de Mesquita (UFVJM) for potentiometric titration analyses.

Appendix A. Supplementary data

Supplementary data to this article can be found online at https://doi.org/10.1016/j.jenvman.2020.111685.

References

Ahmad, M., Rajapaksha, A.U., Lim, J.E., Zhang, M., Bolan, N., Mohan, D., Vithanage, M., Lee, S.S., Ok, Y.S., 2014. Biochar as a sorbent for contaminant management in soil and water: a review. Chemosphere 99, 19–33. https://doi.org/10.1016/j.chemosphere.2013.10.071.

Alves, L.A., De Castro, A.H., De Mendonça, F.G., De Mesquita, J.P., 2016. Characterization of acid functional groups of carbon dots by nonlinear regression

data fitting of potentiometric titration curves. Appl. Surf. Sci. 370, 486–495. https://doi.org/10.1016/j.apsusc.2016.02.128.
Archanjo, B.S., Araujo, J.R., Silva, A.M., Capaz, R.B., Falcão, N.P.S., Jorio, A., Achete, C. A., 2014. Chemical analysis and molecular models for calcium–oxygen–carbon interactions in black carbon found in fertile amazonian anthrosoils. Environ. Sci. Technol. 48, 7445–7452. https://doi.org/10.1021/es501046b.
Archanjo, B.S., Baptista, D.L., Sena, L.A., Cançado, L.G., Falcão, N.P.S., Jorio, A., Achete, C.A., 2015. Nanoscale mapping of carbon oxidation in pyrogenic black carbon from ancient Amazonian anthrosols. Environ. Sci. Process. Impacts 17, 775–779. https://doi.org/10.1039/C4EM00590B.
Bai, T., Qu, W., Yan, Y., Ma, K., Xu, Yonggang, Zhou, X., Chen, Y., Xu, Yingyi, 2020. Influence of pyrolysis temperature on the properties and environmental safety of heavy metals in chicken manure-derived biochars. J. Environ. Sci. Heal. https://doi.org/10.1080/03601234.2020.1797424. Part B 1–10.
Barrera, D., De Mendonça, F.G., De Castro, A.H., De Mesquita, J.P., Lago, R.M., Sapag, K., 2018. Surface modified mesoporous nanocast carbon as a catalyst for aqueous sulfide oxidation and adsorption of the produced polysulfides. New J. Chem. 42, 11708–11714. https://doi.org/10.1039/C8NJ00922H.
Bashir, M.A., Naveed, M., Ahmad, Z., Gao, B., Mustafa, A., Núñez-Delgado, A., 2020. Combined application of biochar and sulfur regulated growth, physiological, antioxidant responses and Cr removal capacity of maize (Zea mays L.) in tannery polluted soils. J. Environ. Manag. 259, 110051. https://doi.org/10.1016/j.jenvman.2019.110051.
Bezerra, J., 2015. In: Bezerra, J. (Ed.), Terra Preta de Índio and Amazonian History BT - The Brazilian Amazon: Politics, Science and International Relations in the History of the Forest. Springer International Publishing, Cham, pp. 15–58. https://doi.org/10.1007/978-3-319-23030-6_2.
Boguta, P., Sokołowska, Z., Skic, K., Tomczyk, A., 2019. Chemically engineered biochar – effect of concentration and type of modifier on sorption and structural properties of biochar from wood waste. Fuel 256, 115893. https://doi.org/10.1016/j.fuel.2019.115893.
Braga, F.M., Barbosa, M.H.C., Oliveira, E.S.A., Sousa, I. de P., Santos, C.B. dos, Sampaio, R.A., 2020. Physical and chemical characterization of sewage sludge with different proportions of diatomaceous earth. Rev. Ceres 67, 81–85. https://doi.org/10.1590/0034-737x202067010011.
Campos, J.L.E., Miranda, H., Rabelo, C., Sandoz-Rosado, E., Pandey, S., Riikonen, J., Cano-Marquez, A.G., Jorio, A., 2018. Applications of Raman spectroscopy in graphene-related materials and the development of parameterized PCA for large-scale data analysis. J. Raman Spectrosc. 49, 54–65. https://doi.org/10.1002/jrs.5225.
Chen, H., Li, W., Wang, J., Xu, H., Liu, Y., Zhang, Z., Li, Y., Zhang, Y., 2019. Adsorption of cadmium and lead ions by phosphoric acid-modified biochar generated from chicken feather: selective adsorption and influence of dissolved organic matter. Bioresour. Technol. 292, 121948. https://doi.org/10.1016/j.biortech.2019.121948.
Chen, Q., Zheng, J., Zheng, L., Dang, Z., Zhang, L., 2018. Classical theory and electron-scale view of exceptional Cd(II) adsorption onto mesoporous cellulose biochar via experimental analysis coupled with DFT calculations. Chem. Eng. J. 350, 1000–1009. https://doi.org/10.1016/j.cej.2018.06.054.
Chen, T., Luo, L., Deng, S., Shi, G., Zhang, S., Zhang, Y., Deng, O., Wang, L., Zhang, J., Wei, L., 2018. Sorption of tetracycline on H_3PO_4 modified biochar derived from rice straw and swine manure. Bioresour. Technol. 267, 431–437. https://doi.org/10.1016/j.biortech.2018.07.074.
CONAMA, 2006. Ministério do Meio Ambiente. Conselho Nacional de Meio Ambiente. Resolução n. 375. de 29 de agosto de 2006. Define critérios e procedimentos, para o uso agrícola de lodos de esgoto gerados em estações de tratamento de esgoto sanitário e seus produtos deri, pp. 555–579.
Cuong, D.V., Liu, N.-L., Nguyen, V.A., Hou, C.-H., 2019. Meso/micropore-controlled hierarchical porous carbon derived from activated biochar as a high-performance adsorbent for copper removal. Sci. Total Environ. 692, 844–853. https://doi.org/10.1016/j.scitotenv.2019.07.125.
de la Puente, G., Pis, J.J., Menéndez, J.A., Grange, P., 1997. Thermal stability of oxygenated functions in activated carbons. J. Anal. Appl. Pyrolysis 43, 125–138. https://doi.org/10.1016/S0165-2370(97)00060-0.
Dominguez, E.L., Uttran, A., Loh, S.K., Manero, M.-H., Upperton, R., Idris Tanimu, M., Thomas Bachmann, R., 2020. Characterisation of industrially produced oil palm kernel shell biochar and its potential as slow release nitrogen-phosphate fertilizer and carbon sink. Mater. Today Proc. https://doi.org/10.1016/j.matpr.2020.05.143.
El-Banna, M.F., Mosa, A., Gao, B., Yin, X., Ahmad, Z., Wang, H., 2018. Sorption of lead ions onto oxidized bagasse-biochar mitigates Pb-induced oxidative stress on hydroponically grown chicory: experimental observations and mechanisms. Chemosphere 208, 887–898. https://doi.org/10.1016/j.chemosphere.2018.06.052.
Filgueiras, O., 2007. Silício na agricultura. Pesqui. Fapesp 72–74.
Gámiz, B., Velarde, P., Spokas, K.A., Cox, L., 2019. Dynamic effect of fresh and aged biochar on the behavior of the herbicide mesotrione in soils. J. Agric. Food Chem. 67, 9450–9459. https://doi.org/10.1021/acs.jafc.9b02618.
Glaser, B., Birk, J.J., 2012. State of the scientific knowledge on properties and genesis of Anthropogenic Dark Earths in Central Amazonia (terra preta de Índio). Geochem. Cosmochim. Acta 82, 39–51. https://doi.org/10.1016/j.gca.2010.11.029.
Glaser, B., Haumaier, L., Guggenberger, G., Zech, W., 2001. The "Terra Preta" phenomenon: a model for sustainable agriculture in the humid tropics. Naturwissenschaften 88, 37–41. https://doi.org/10.1007/s001140000193.
Huber, G.W., Iborra, S., Corma, A., 2006. Synthesis of transportation fuels from Biomass: chemistry, catalysts, and engineering. Chem. Rev. 106, 4044–4098. https://doi.org/10.1021/cr068360d.
Jaganathan, V.M., Varunkumar, S., 2020. A novel self-sustained single step process for synthesizing activated char from ligno-cellulosic biomass. Fuel Process. Technol. 208, 106516. https://doi.org/10.1016/j.fuproc.2020.106516.
Jorio, A., Ribeiro-Soares, J., Cançado, L.G., Falcão, N.P.S., Dos Santos, H.F., Baptista, D. L., Martins Ferreira, E.H., Archanjo, B.S., Achete, C.A., 2012. Microscopy and spectroscopy analysis of carbon nanostructures in highly fertile Amazonian anthrosoils. Soil Tillage Res. 122, 61–66. https://doi.org/10.1016/j.still.2012.02.009.
Jorio, A., Saito, R., Dresselhaus, G., Dresselhaus, M.S., 2011. Raman Spectroscopy in Graphene Related Systems. WILEY-VCH Verlag GmbH & Co. KGaA, Weinheim, ISBN 978-3-527-40811-5. https://doi.org/10.1103/PhysRevD.64.084027.
Kan, T., Strezov, V., Evans, T.J., 2016. Lignocellulosic biomass pyrolysis: a review of product properties and effects of pyrolysis parameters. Renew. Sustain. Energy Rev. 57, 1126–1140. https://doi.org/10.1016/j.rser.2015.12.185.
Kavitha, B., Reddy, P.V.L., Kim, B., Lee, S.S., Pandey, S.K., Kim, K.-H., 2018. Benefits and limitations of biochar amendment in agricultural soils: a review. J. Environ. Manag. 227, 146–154. https://doi.org/10.1016/j.jenvman.2018.08.082.
Lemos, B.R.S., Teixeira, I.F., Machado, B.F., Alves, M.R.A., de Mesquita, J.P., Ribeiro, R. R., Bacsa, R.R., Serp, P., Lago, R.M., 2013. Oxidized few layer graphene and graphite as metal-free catalysts for aqueous sulfide oxidation. J. Mater. Chem. A 1, 9491–9497. https://doi.org/10.1039/C3TA10541E.
Lipens, B., Linsen, B., Boer, J.H.D., 1964. Studies on pore systems in catalysts I: the adsorption of nitrogen; aparatus and calculation. J. Catal. 3, 32–37.
Ma, J., Zhou, B., Zhang, H., Zhang, W., Wang, Z., 2019. Activated municipal wasted sludge biochar supported by nanoscale Fe/Cu composites for tetracycline removal from water. Chem. Eng. Res. Des. 149, 209–219. https://doi.org/10.1016/j.cherd.2019.07.013.
Malavolta, E., 2006. Manual de nutrição mineral de plantas. São Paulo: agronômica Ceres. Embrapa Acre; Embrapa Meio Ambient. Embrapa Semiárido 638p.
Martínez-Casillas, D.C., Alonso-Lemus, I.L., Mascorro-Gutiérrez, I., Cuentas-Gallegos, A. K., 2018. Leather waste-derived biochar with high performance for supercapacitors. J. Electrochem. Soc. 165, A2061–A2068. https://doi.org/10.1149/2.0421810jes.
Pagano, M.C., Ribeiro-Soares, J., Cançado, L.G., Falcão, N.P.S., Gonçalves, V.N., Rosa, L. H., Takahashi, J.A., Achete, C.A., Jorio, A., 2016. Depth dependence of black carbon structure, elemental and microbiological composition in anthropic Amazonian dark soil. Soil Tillage Res. 155, 298–307. https://doi.org/10.1016/j.still.2015.09.001.
Ribeiro-Soares, J., Cançado, L.G., Falcão, N.P.S., Martins Ferreira, E.H., Achete, C.A., Jorio, A., 2013. The use of Raman spectroscopy to characterize the carbon materials found in Amazonian anthrosoils. J. Raman Spectrosc. 44, 283–289. https://doi.org/10.1002/jrs.4191.
Salam, A., Bashir, S., Khan, I., Hu, H., 2020. Biochar production and characterization as a measure for effective rapeseed residue and rice straw management: an integrated spectroscopic examination. Biomass Convers. Biorefinery. https://doi.org/10.1007/s13399-020-00820-z.
Santos, N.A.V., Vieira, S.S., Mendonça, F.G., Napolitano, M.N., Nunes, D.M., Ferreira, R. A.R., Soares, R.R., Magriotis, Z.M., Araujo, M.H., Lago, R.M., 2017. Rejeitos de Biomassas Oriundas da Cadeia de Biocombustíveis no Brasil: produção de Bio-óleo e Sub-produtos. Rev. Virtual Quim. https://doi.org/10.21577/1984-6835.20170007.
Shang, L., Xu, H., Huang, S., Zhang, Y., 2018. Adsorption of ammonium in aqueous solutions by the modified biochar and its application as an effective N-fertilizer. Water, air. Soil Pollut 229, 320. https://doi.org/10.1007/s11270-018-3956-1.
Sharma, A., Weindorf, D.C., Wang, D., Chakraborty, S., 2015. Characterizing soils via portable X-ray fluorescence spectrometer: 4. Cation exchange capacity (CEC). Geoderma 239–240, 130–134. https://doi.org/10.1016/j.geoderma.2014.10.001.
Suliman, W., Harsh, J.B., Abu-Lail, N.I., Fortuna, A.M., Dallmeyer, I., Garcia-Perez, M., 2016. Influence of feedstock source and pyrolysis temperature on biochar bulk and surface properties. Biomass Bioenergy 84, 37–48. https://doi.org/10.1016/j.biombioe.2015.11.010.
Sullivan, G.L., Prigmore, R.M., Knight, P., Godfrey, A.R., 2019. Activated carbon biochar from municipal waste as a sorptive agent for the removal of polyaromatic hydrocarbons (PAHs), phenols and petroleum based compounds in contaminated liquids. J. Environ. Manag. 251, 109551. https://doi.org/10.1016/j.jenvman.2019.109551.
Sun, K., Huang, Q., Ali, M., Chi, Y., Yan, J., 2018. Producing aromatic-enriched oil from mixed plastics using activated biochar as catalyst. Energy Fuels 32, 5471–5479. https://doi.org/10.1021/acs.energyfuels.7b03710.
Tedesco, M.J., Gianello, C., Bissani, C.A., Bohnen, H., Volkweiss, S.J., 1995. Análise de solo, plantas e outros materiais, 2. Porto Alegre: UFRGS, Departamento de solos.
Thommes, M., Kaneko, K., Neimark, A.V., Olivier, J.P., Rodriguez-Reinoso, F., Rouquerol, J., Sing, K.S.W., 2015. Physisorption of gases, with special reference to the evaluation of surface area and pore size distribution (IUPAC Technical Report). Pure Appl. Chem. 87, 1051–1069.
Wang, He, Wang, Han, Zhao, H., Yan, Q., 2020. Adsorption and Fenton-like removal of chelated nickel from Zn-Ni alloy electroplating wastewater using activated biochar composite derived from Taihu blue algae. Chem. Eng. J. 379, 122372. https://doi.org/10.1016/j.cej.2019.122372.
Wang, Y., Dong, H., Li, L., Tian, R., Chen, J., Ning, Q., Wang, B., Tang, L., Zeng, G., 2019. Influence of feedstocks and modification methods on biochar's capacity to activate hydrogen peroxide for tetracycline removal. Bioresour. Technol. 291, 121840. https://doi.org/10.1016/j.biortech.2019.121840.

Xiao, Z., Rasmann, S., Yue, L., Lian, F., Zou, H., Wang, Z., 2019. The effect of biochar amendment on N-cycling genes in soils: a meta-analysis. Sci. Total Environ. 696, 133984. https://doi.org/10.1016/j.scitotenv.2019.133984.

Yang, H., Yan, R., Chen, H., Zheng, C., Lee, D.H., Liang, D.T., 2006. In-depth investigation of biomass pyrolysis based on three major components: hemicellulose, cellulose and lignin. Energy Fuels 20, 388–393. https://doi.org/10.1021/ef0580117.

Zelaya, K.P.S., Alves, B.S.Q., Colen, F., Frazão, L.A., Sampaio, R.A., Pegoraro, R.F., Fernandes, L.A., 2019. Biochar in sugar beet production and nutrition. Ciência Rural. 49 https://doi.org/10.1590/0103-8478cr20180684.